Structural Eng./Earthquake Eng., JSCE, Vol. 21, No. 2, 143s - 158s, 2004 October
(J. Struct. Mech. Earthquake Eng., JSCE, No. 733/ I - 69)

A NUMERICAL METHOD FOR WAVE SCATTERING IN POROELASTIC MEDIA

Koji YAMAMOTO[1] and Michihiro KITAHARA[2]

[1]Member of JSCE, Dept. of Civil Eng., Tohoku University (Aoba 6-6-06, Sendai 980-8579, JAPAN)
E-mail : yamamoto@nde.civil.tohoku.ac.jp
[2]Member of JSCE, Dr.Eng., Professor, Dept. of Civil Eng., Tohoku University
(Aoba 6-6-06, Sendai 980-8579, JAPAN)

Wave scattering in the Biot's poroelastic media is investigated using a numerical method based on the boundary integral formulation. The formulation adopts the fundamental solution derived with a direct manner and traction operators for physically meaningful boundary conditions. Some numerical examples for wave incidence on a spherical scatterer is presented. In the examples, coupling effects of solid and fluid are parameterized with coupling parameters and the boundary conditions. The results show that scattered fields, especially pore pressure, are highly influenced by the coupling effects with the conversion of the fast longitudinal wave to the slow one.

Key Words : *poroelasticity, wave scattering, Biot's material, boundary integral equation*

1. INTRODUCTION

Based on the three-dimensional model of poroelasticity,[1] Biot developed a theory of wave propagation in fluid saturated porous media.[2),3)] Some important characters of waves in the Biot's model are 1) the existence of two dilatational waves as well as the transverse wave, and 2) energy dissipation due to the relative motion between fluid and solid. The latter leads to the dispersion of phase velocity and attenuation of the waves.

The Biot's theory of poroelasticity has been investigated in various application field such as geophysical exploration,[4)] rock engineering,[5)] and biomechanics.[6)] As a numerical method for dynamic poroelasticity, the finite difference method (FDM) was developed for the wave propagation in geophysical applications by Hassanzadeh.[7)] The thin layered element models were adopted for the earthquake response of layered formations by Kazama and Nogami,[8)] Kitamura and Asai,[9)] and Takano *et al.*[10),11)]

The boundary element method (BEM) is another possible method for the dynamic problems. The quasi-static time domain BEM is used to analyze the soil consolidation problem.[12)] The frequency domain BEMs were formulated for the wave problems by Cheng *et al.*[13)] and Dominguez.[14)] In the studies, the fundamental solution for the dynamic poroelasticity is derived with the analogy to the thermoelasticity. However, results of wave scatterings by a scatterer were not presented explicitly. Fukui *et al.*[15)] formulated the two-dimensional BEM for the wave scattering problem using the poroelastic parameters in the Biot's first paper of dynamic poroelasticity[2)] with independently derived two-dimensional fundamental solution. Also some numerical solutions of BEM were presented on the cavity surface. In the study, however, physical meaning of the boundary condition of fluid part is not clear due to the structure of its traction operator and parameters used. As some specific applications of the frequency domain BEM, the earthquake response of a structure on a fluid filled half-space under undrained condition was modeled with BEM by Utsumi *et al.*[16)] The wave propagation induced by a surface load in the half-space was studied by Kitamura *et al.*[17)] using BEM formulations.

Our final target is to apply the wave scattering theory to exploration geophysics and nondestructive evaluation in fluid saturated earth materials. For this purpose, we utilize the frequency domain BEM for the problem of wave scattering in poroelastic materials to understand the nature of scattered waves by a scatterer embedded in porous materials. The characteristics of the scattered field, especially the effect of poroelastic parameters on the scattered field give us the information for better interpretation of measured scattered waves. The BEM has an advantage for

the problem in infinite media, and useful for such wave scattering analysis.

This paper presents the boundary integral equation for the scattering problem with physically meaningful boundary conditions using poroelastic parameters in a later work of Biot.[3] In the formulation, the surface condition is permeable or impermeable for the fluid, and the displacement fixed or total traction free condition for the solid part.

In the next section, the basic characteristics of the waves in Biot's material are discussed after showing the governing equations. Then the three-dimensional fundamental solution and the boundary integral equations for poroelastic medium are presented in Sections 3 and 4, respectively. In Section 5, displacement and fluid pressure are computed in the surrounding space of the scatterer as well as on the scatterer surface in order to examine the coupling effects on the scattered waves. Mainly, effects of two poroelastic parameters related to the coupling behavior between solid and fluid are discussed to evaluate the characteristics of the coupled system. Also, the effects of frequency and boundary conditions are investigated.

2. WAVE PROPAGATION IN POROELASTIC MEDIA

(1) Governing equations

The fundamental equations in the Biot's poroelastic theory are summarized for the subsequent use.

The medium in the Biot's model is a bulk material that consists of a porous solid frame formed by impervious solid grains and pores, and a single-phase compressible fluid saturating the pore spaces. The sizes of the grains and pores are distributed around the average values, and small enough compared with the wavelength. Therefore, we regard the medium as a macroscopically continuous and homogeneous mixture.

The displacements of solid and fluid, denoted by u_i and U_i respectively, are defined separately in the medium, as shown in **Fig.1**. The strain tensor of the solid frame e_{ij} is denoted by

$$e_{ij} = \frac{1}{2}\left(u_{i,j} + u_{j,i}\right). \tag{1}$$

The subscripts i and j indicate the spatial components, and their range is 1 to 3.

The fluid volume that passes through a unit area of the solid frame in x_i-direction is designated by w_i, and given from the relative motion of fluid and solid:

$$w_i = \beta\left(U_i - u_i\right) \tag{2}$$

where β is the porosity of the medium.

When the medium is isotropic, and the stress-strain relation is linear, the constitutive relations of the fluid-solid coupled system are written as follows[3]:

$$\sigma_{ij} = 2\mu e_{ij} + (\lambda e - \alpha p)\,\delta_{ij} \tag{3}$$

$$p = -\alpha M e + M\zeta \tag{4}$$

where σ_{ij} represents the total stress, $e = e_{kk}$ is the volumetric strain of the solid frame, p is the pore pressure, $\zeta = -w_{k,k}$ is the quantity of fluid that enters a unit volume of the solid frame, and δ_{ij} is the Kronecker's delta.

Four independent elastic constants appear in Eqs.(3) and (4). Here μ and λ are Lamé constants of the solid frame without any effect of the pore fluid ($p = 0$). The constant α is the Biot's constant (Biot-Willis coefficient). Biot's modulus M represents the pore pressure increase per unit increase of fluid content under no volumetric strain condition ($e = 0$).[18] The physical meanings of α and M are described later.

The equation of motion for the bulk material is written as

$$\sigma_{ij,j} + \rho b_i = (\rho - \beta\rho_f)\ddot{u}_i + \beta\rho_f\ddot{U}_i = \rho\ddot{u}_i + \rho_f\ddot{w}_i \tag{5}$$

where ρ and ρ_f are densities of the bulk material and the pore fluid, respectively. The body force acting on the bulk material is denoted by b_i.

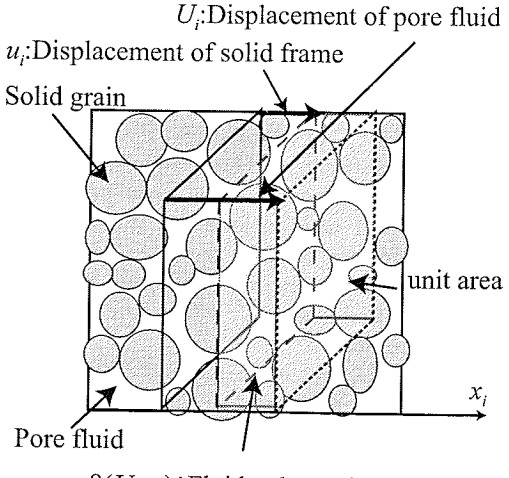

Fig. 1 Displacements of solid frame (u_i) and fluid (U_i), and relative fluid motion in volume w_i

For the equation of motion for the fluid part, friction loss of the pressure caused by inter pore flow needs to be taken into account.[2] The pressure loss $p_i^{(d)}$ is assumed to be governed by the generalized Darcy's law

$$\dot{w}_i = -\frac{k}{\eta} p_{,i}^{(d)} \tag{6}$$

where k is the permeability of the medium, and η is the viscosity of the fluid. Thus the equations of motion of the fluid part[3] is written as follows:

$$p_{,i} + \rho_f c_i = -\rho_f \ddot{U}_i + p_{,i}^{(d)} = -\rho_f \ddot{u}_i - \frac{\rho_f}{\beta}\ddot{w}_i - \frac{\eta}{k}\dot{w}_i \tag{7}$$

where c_i is the body force acting on the fluid part.

For a time-harmonic wave propagation with an angular frequency ω, the equations of motion are reduced to

$$\sigma_{ij,j} + \rho b_i = -\omega^2(\rho u_i + \rho_f w_i) \tag{8}$$

$$p_{,i} + \rho_f c_i = \omega^2(\rho_f u_i + \tilde{m} w_i) \tag{9}$$

where the time factor $e^{-i\omega t}$ is suppressed. In Eqs.(8) and (9), the complex mass parameter $\tilde{m}$ is introduced as follows:

$$\tilde{m} = m + i\frac{b}{\omega} \tag{10}$$

where the mass parameter m and the dissipation parameter b defined as

$$m = \frac{\rho_f}{\beta},\ b = \frac{\eta}{k}. \tag{11}$$

The imaginary part of the mass parameter $\tilde{m}$ implies the dissipation effect of the material.

We choose the solid displacement u_i and the pore pressure p as variables to be solved. The terms of σ_{ij} and the relative fluid motion w_i are eliminated from Eq.(8) and divergence of Eq.(9) using constitutive relations in Eqs.(3) and (4), and a poroelastic counterpart of the Navier-Cauchy equation is reduced to

$$\mu u_{i,jj} + (\lambda+\mu)u_{j,ji} + w^2\tilde{\rho}u_i - \tilde{\alpha}p_{,i} = -\left(\rho b_i + \frac{\rho_f^2}{\tilde{m}}c_i\right) \tag{12}$$

$$\frac{1}{\omega^2\tilde{m}}p_{,ii} + \frac{1}{M}p + \tilde{\alpha}u_{i,i} = -\frac{\rho_f}{\omega^2\tilde{m}}c_{i,i} \tag{13}$$

where the complex mass and poroelastic parameters $\tilde{\rho}$ and $\tilde{\alpha}$ are introduced as follows:

$$\tilde{\rho} = \rho - \frac{\rho_f^2}{\tilde{m}},\ \tilde{\alpha} = \alpha - \frac{\rho_f}{\tilde{m}}. \tag{14}$$

The right-hand-sides in Eqs.(12) is the body causing total stress. Eq.(13) has a form of the equation of continua in which the first term of the left-hand-side is the fluid motion and the second and third terms are elastic strain of fluid due to its compressibility and the coupled effect of solid strain, respectively. The right-hand-side is the body force in fluid that works as a pressure source.

Eqs.(12) and (13) are rewritten in a matrix form:

$$L_{IJ}q_J = -\mathcal{B}_I \tag{15}$$

where

$$L_{IJ} = \begin{bmatrix} L_{ij} & L_{i4} \\ L_{4j} & L_{44} \end{bmatrix} = \begin{bmatrix} \partial_k C_{kilj}\partial_l + \omega^2\tilde{\rho}\delta_{ij} & -\tilde{\alpha}\partial_i \\ \tilde{\alpha}\partial_j & \frac{1}{\omega^2\tilde{m}}\triangle + \frac{1}{M} \end{bmatrix}. \tag{16}$$

In this expression, operators $\partial_i = \partial/\partial x_i$, $C_{kilj} = \lambda\delta_{ki}\delta_{lj} + \mu(\delta_{kl}\delta_{ij} + \delta_{kj}\delta_{li})$ are used. Another operator $\triangle$ denotes the Laplacian ($\triangle = \nabla\cdot\nabla$). In Eq.(15), q_J denotes the generalized displacement that consists of three solid displacement components and the fluid pressure term, as follows

$$\boldsymbol{q} = \{u_j, p\}^T. \tag{17}$$

$\mathcal{B}_I$ is the body force term and written as

$$\boldsymbol{\mathcal{B}} = \left\{\rho b_i + \frac{\rho_f^2}{\tilde{m}}c_i, \frac{\rho_f}{\omega^2\tilde{m}}c_{k,k}\right\}^T. \tag{18}$$

The range of the subscripts in capital letters I, J is 1 to 4, in which 1 to 3 denote the quantities in spatial coordinates and 4 is the fluid pressure term.

(2) Waves in Biot's material

Here we consider a time harmonic plane wave that propagates along the x_1 axis with the wavenumber k. Displacement components and pressure of the wave are denoted as

$$\{u_i, p\} = \left\{A_i e^{ikx_1}, Be^{ikx_1}\right\}. \tag{19}$$

By substituting Eq.(19) into Eq.(15) without body forces, and omitting the factor e^{ikx_1}, the characteristic equation for the waves is given as follows:

$$\begin{bmatrix} h_1 & 0 & 0 & ik\tilde{\alpha} \\ 0 & h_2 & 0 & 0 \\ 0 & 0 & h_2 & 0 \\ -ik\tilde{\alpha} & 0 & 0 & h_3 \end{bmatrix} \begin{Bmatrix} A_1 \\ A_2 \\ A_3 \\ B \end{Bmatrix} = \begin{Bmatrix} 0 \\ 0 \\ 0 \\ 0 \end{Bmatrix} \tag{20}$$

where

$$h_1 = (\lambda + 2\mu)k^2 - \omega^2\tilde{\rho} \tag{21}$$

$$h_2 = \mu k^2 - \omega^2\tilde{\rho} \tag{22}$$

$$h_3 = \frac{k^2}{\omega^2\tilde{m}} - \frac{1}{M}. \tag{23}$$

For the tranverse waves ($I = 2, 3$), the wavenumber k should satisfy the equation:

$$h_2 = 0 \tag{24}$$

then the wavenumber k_T for the transverse wave is derived as

$$k_T^2 = \frac{\tilde{\rho}}{\mu}\omega^2. \tag{25}$$

For the longitudinal waves, the solid displacement ($I = 1$) and fluid pressure ($I = 4$) are coupled through the terms with the complex parameter $\tilde{\alpha}$, and the wavenumber k should satisfy the characteristic equation

$$h_1 h_3 - k^2\tilde{\alpha}^2 = 0 \tag{26}$$

then the equation is rewritten as

$$\frac{\lambda + 2\mu}{\omega^2\tilde{m}}\left(k^2 - \frac{\omega^2\tilde{\rho}}{\lambda + 2\mu}\right)\left(k^2 - \frac{\omega^2\tilde{m}}{M}\right) - k^2\tilde{\alpha}^2 = 0. \tag{27}$$

We introduce the wavenumbers defined by Fukui *et al.*[15] denoted by

$$k_{L1_0}^2 = \frac{\tilde{\rho}}{\lambda + 2\mu}\omega^2, \quad k_{L2_0}^2 = \frac{\tilde{m}}{M}\omega^2,$$
$$\text{and } k_Q^2 = \frac{\tilde{m}\tilde{\alpha}^2}{\lambda + 2\mu}\omega^2. \tag{28}$$

Since k_{L1_0} and k_{L2_0} are the solutions of Eq.(26) in the case that the coupling parameter $\tilde{\alpha}$ is zero, these are regarded as wavenumbers of pure solid and fluid waves without the coupling effect. The wavenumber k_Q represents the intensity of the coupling effect. Using those wavenumbers, Eq.(27) is rewritten as

$$\frac{\lambda + 2\mu}{\omega^2\tilde{m}}\left\{(k^2 - k_{L1_0}^2)(k^2 - k_{L2_0}^2) - k_Q^2 k^2\right\} = 0. \tag{29}$$

Therefore, the wavenumbers for the coupled longitudinal waves are obtained as

$$\left.\begin{matrix} k_{L1}^2 \\ k_{L2}^2 \end{matrix}\right\} = \frac{1}{2}\left[(k_{L2_0}^2 + k_{L1_0}^2 + k_Q^2) \mp \left\{(k_{L2_0}^2 + k_{L1_0}^2 + k_Q^2)^2 - 4k_{L1_0}^2 k_{L2_0}^2\right\}^{\frac{1}{2}}\right]. \tag{30}$$

These two longitudinal waves with wavenumbers k_{L1} and k_{L2} correspond to the Biot's compressional waves in the first and the second kind,[2] respectively. We simply call these waves as $L1$-wave and $L2$-wave.

To satisfy Eq.(20), the amplitude ratios of solid displacement and fluid pressure for the $L1$ and the $L2$-wave $(A_1/B)_{L1}$ and $(A_1/B)_{L2}$ should satisfy the following relations:

$$\left(\frac{A_1}{B}\right)_{L1} = i\frac{k_{L1}}{k_{L1_0}^2 - k_{L1}^2}\frac{\tilde{\alpha}}{\lambda + 2\mu} \tag{31}$$

$$\left(\frac{A_1}{B}\right)_{L2} = -i\frac{k_{L2}^2 - k_{L2_0}^2}{k_{L2}k_Q^2}\frac{\tilde{\alpha}}{\lambda + 2\mu}. \tag{32}$$

(3) Basic characters of the waves

Some characters of the waves in the poroelastic media are summarized. The coupling effect between solid displacements and fluid pressure is governed by two dimensionless parameters; the poroelastic constant α and the dimensionless dissipation factor $b/(m\omega)$.

Among four elastic parameters appearing in constitutive relations Eqs.(3) and (4), λ and μ are the parameters of solid frame without fluid. The other two parameters govern the effects of pore fluid on the dynamic behavior of the material. Other combination of the parameters can be used,[2),19] but we chose those parameters because their physical meanings are clear, and they can be measured or evaluated from the elastic parameters of constituents of the media. Specifically, the effect of fluid compressibility is easily understood using those parameters. As shown in Eq.(4), Biot's modulus M denotes the pressure change caused by the deformation of solid frame and fluid inflow to pore spaces. In the case that the compressibility of the solid grain is significantly lower than the solid frame, M can be written as $M \sim K_f/\beta$ where K_f is the bulk modulus of the pore fluid,[20] then it represents the effect of the fluid deformation on the pressure.

Biot's constant α takes a value between the porosity and one ($\beta \leq \alpha \leq 1.0$). The complex parameter $\tilde{\alpha}$ indicates the intensity of the coupling effect. When both α and $b/(m\omega)$ take the smallest value ($\alpha = \beta$ and $b/(m\omega) = 0$), the value of $\tilde{\alpha}$ is zero, and the longitudinal waves in solid frame and fluid propagate independently with wavenumbers $L1_0$ and $L2_0$ defined in Eqs.(28).

Generally, in granular materials such as sandstone, α takes a value close to 1.0 and relatively small value of b due to their high porosity and permeability. In crystalline materials such as granite, value of α is small and close to β, and b is relatively large. Mechanisms which determine the

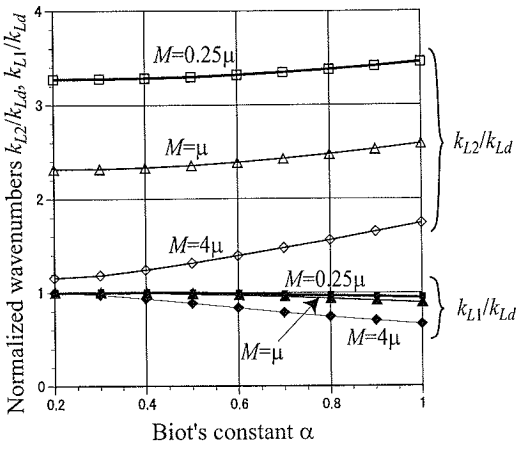

Fig. 2 Variation of the wavenumbers k_{L2}, k_{L1} with different poroelastic parameters α and M. ($\beta = 0.2$, $\lambda = \mu$ ($\nu = 0.25$), no dissipation cases :$b/(m\omega) = 0$)

value of α was well discussed by Skempton.[21] The values of such poroelastic parameters in some specific rocks appear in Detournay and Cheng.[5]

The effect of the coupling parameter α on the wavenumbers of the longitudinal waves is investigated for the no dissipation case ($b/(m\omega) = 0$). To normalize the wavenumbers, we use the wavenumber k_{Ld} of the wave in solid frame without fluid. k_{Ld} is written as

$$k_{Ld}^2 = (\rho - \rho_f\beta)\omega^2/(\lambda + 2\mu). \qquad (33)$$

Fig.2 shows the normalized longitudinal wavenumbers as a function of α for various values M. Other parameters are set to be $\beta = 0.2$, $\mu = \lambda(\nu = 0.25)$ and $\rho = 3\rho_f$ as typical values of sandstones.[5]

When α approaches to the porosity ($\alpha \to \beta = 0.2$), k_{L1} agrees with k_{Ld}. As α increases, k_{L1} decreases so that the velocity of $L1$-wave is increased. On the other hand, as α increases, k_{L2} monotonically increases and then the wave velocity is decreased. Therefore the difference of two longitudinal wave velocities is more significant for higher values of α.

The effects of the other coupling parameter $b/(m\omega)$ on the $L1$- and $L2$-waves are illustrated in **Fig.3** and **Fig.4**, respectively. In **Fig.3**, k_{Lw} denotes the wavenumber of the wave in which the fluid mass influences the wave velocity, and written as

$$k_{Lw}^2 = \rho\omega^2/(\lambda + 2\mu). \qquad (34)$$

Fig.3 shows that $L1$-wave is not dissipative because the imaginary part of k_{L1} is very small.

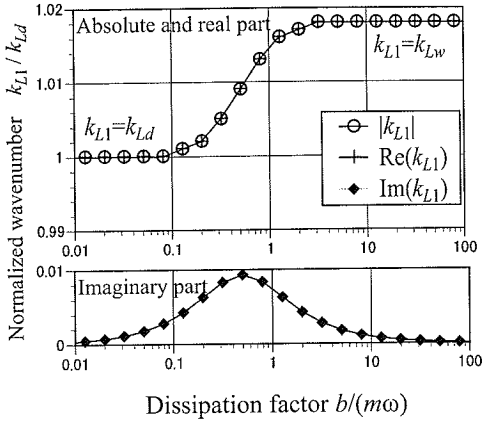

Fig. 3 Variation of the wavenumber k_{L1} with different dissipation factor $b/(m\omega)$. ($\beta = 0.2$, $\lambda = \mu$ ($\nu = 0.25$), $\alpha = 0.6$)

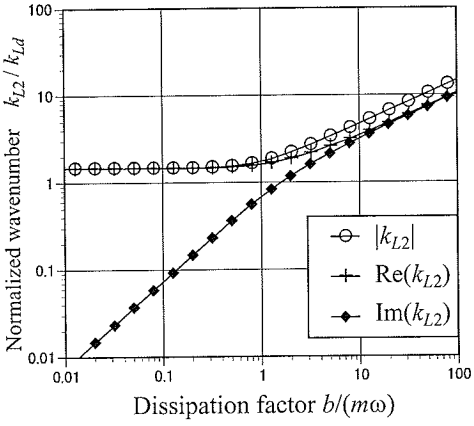

Fig. 4 Variation of the wavenumber k_{L2} with different dissipation factor $b/(m\omega)$. ($\beta = 0.2$, $\lambda = \mu$ ($\nu = 0.25$), $\alpha = 0.6$)

When dissipation is negligible ($b/(m\omega) \ll 1$), the real part of k_{L1} coincides with k_{Ld}. At the high dissipation limit ($b/(m\omega) \gg 1$), k_{L1} matches with the wavenumber k_{Lw}.

The effect of $b/(m\omega)$ on the $L2$-wave is more significant than that on the $L1$-wave, and wave velocity of the $L2$-wave is significantly slow and highly dissipating when the dissipation factor is larger than 1.

3. FUNDAMENTAL SOLUTIONS FOR POROELASTIC MEDIA

The frequency domain fundamental solution for three-dimensional poroelasticity has been derived by Cheng *et al.*[13] and Dominguez.[14] They adopted the analogy between thermoelasticity

and poroelasticity, and gave the solution from a known solution for thermoelasticity. Here, we derive an explicit form of the solution with a direct manner using the Fourier transform and ensure that the derived solution agrees with the previous works. The two-dimensional fundamental solution was given by Fukui *et al.*[15] by the same manner but using poroelastic parameter of Biot.[2]

The fundamental solution G_{JK} for Eq.(15) is defined as

$$L_{IJ}G_{JK}(\boldsymbol{x},\boldsymbol{y}) = -\delta_{IK}\delta(\boldsymbol{x}-\boldsymbol{y}). \tag{35}$$

The Fourier transform in the three-dimensional space is

$$\begin{aligned}\hat{f}(\boldsymbol{\xi}) &= F[f(\boldsymbol{x})] \\ &= \int\int\int_{-\infty}^{\infty} f(\boldsymbol{x})e^{-i\boldsymbol{\xi}\cdot\boldsymbol{x}}d\boldsymbol{x}.\end{aligned} \tag{36}$$

Using the nature of the Fourier transorm $F[\delta(\boldsymbol{x}-\boldsymbol{y})] = e^{-i\boldsymbol{\xi}\cdot\boldsymbol{y}}$, we get the transformed form of Eq.(35)

$$\hat{L}_{IJ}\hat{G}_{JK} = -\delta_{IK}e^{-i\boldsymbol{\xi}\cdot\boldsymbol{y}} \tag{37}$$

where the Fourier transform of the differential operator $\hat{L}_{IJ}$ is written as

$$\hat{L}_{IJ} = -\begin{bmatrix} a\delta_{ij}+b\xi_i\xi_j & -c\xi_i \\ c\xi_j & d \end{bmatrix} \tag{38}$$

and

$$\begin{aligned} &a = \mu(\xi^2 - k_T^2), \quad b = \lambda+\mu \\ &c = i\tilde{\alpha}, \quad d = \frac{1}{\omega^2\tilde{m}}(\xi^2 - k_{L2_0}^2) \end{aligned} \tag{39}$$

with $\xi^2 = \xi_i\xi_i$. Then the inverse of $\hat{L}_{IJ}$ reduces to

$$\hat{L}_{IJ}^{-1} = -\begin{bmatrix} \dfrac{\delta_{ij}}{a} - \dfrac{(bd+c^2)(\xi_i\xi_j)}{ae} & \dfrac{c\xi_i}{e} \\ -\dfrac{c\xi_j}{e} & \dfrac{a+b\xi^2}{e} \end{bmatrix} \tag{40}$$

where $e = ad + (bd+c^2)\xi^2$.

The fundamental solution G_{IJ} can be obtained in the following form:

$$\begin{aligned} G_{IJ} &= F^{-1}\left[\hat{G}_{IJ}\right] \\ &= F^{-1}\left[-\hat{L}_{IK}^{-1}\delta_{KJ}e^{-i\boldsymbol{\xi}\cdot\boldsymbol{y}}\right]. \end{aligned} \tag{41}$$

Since the factor $i\xi_i$ in the $\boldsymbol{\xi}$-space corresponds to the $\partial/\partial x_i$ in the $\boldsymbol{x}$-space, the explicit expression of the fundamental solution is derived as follows:

$$\begin{aligned} G_{ij} = \frac{1}{4\pi\mu}\Bigg[&\frac{e^{ik_T r}}{r}\delta_{ij} \\ &+K^{12}\frac{\partial}{\partial x_i}\frac{\partial}{\partial x_j}\left\{\frac{k_{L1_0}^2-k_{L2}^2}{k_T^2}\left(\frac{e^{ik_T r}}{r}-\frac{e^{ik_{L1}r}}{r}\right)\right. \\ &\left.-\frac{k_{L1_0}^2-k_{L1}^2}{k_T^2}\left(\frac{e^{ik_T r}}{r}-\frac{e^{ik_{L2}r}}{r}\right)\right\}\Bigg] \end{aligned} \tag{42}$$

$$G_{i4} = -\frac{k_Q^2}{4\pi\tilde{\alpha}}K^{12}\frac{\partial}{\partial x_i}\left(\frac{e^{ik_{L1}r}}{r}-\frac{e^{ik_{L2}r}}{r}\right) \tag{43}$$

$$G_{4i} = \frac{k_Q^2}{4\pi\tilde{\alpha}}K^{12}\frac{\partial}{\partial x_i}\left(\frac{e^{ik_{L1}r}}{r}-\frac{e^{ik_{L2}r}}{r}\right) \tag{44}$$

$$\begin{aligned} G_{44} = &-\frac{M}{4\pi}k_{L2_0}^2K^{12} \\ &\times\left\{(k_{L1_0}^2-k_{L1}^2)\frac{e^{ik_{L1}r}}{r}-(k_{L1_0}^2-k_{L2}^2)\frac{e^{ik_{L2}r}}{r}\right\} \end{aligned} \tag{45}$$

where

$$K^{12} = \frac{1}{k_{L1}^2-k_{L2}^2}. \tag{46}$$

The solid terms G_{ij} have a similar expression to the fundamental solution for elastic media, but include both $L1$- and $L2$- wave components. The fluid term G_{44} is similar to the fundamental solution of the Helmholtz equation with the contributions of both $L1$- and $L2$- waves. The terms G_{i4} and G_{4j} are related to the form of the first derivatives of the fundamental solution for the Helmholtz equation, which show the phase delay of the pressure wave to the elastic wave.

After some manipulations, it can be shown that the solution derived here agrees with the solution of Cheng *et al.* [13] though different poroelastic parameters are used in both solutions.

4. BOUNDARY INTEGRAL EQUATIONS

(1) Reciprocal relation and boundary conditions

For the boundary integral equation for a scattering problem in a poroelastic medium described by the differential equations in Eq.(15), we derive the reciprocal relations with the traction operators that are suitable for the boundary conditions on a cavity surface.

Here, we consider a closed domain D with its boundary S. The body force $\boldsymbol{\mathcal{B}}$ is omitted for simplicity.

For the solid term of the differential operator L_{ij} and the fluid term L_{44}, the reciprocal equations can be written in the following forms

$$\begin{aligned} &\int_D u_i^* L_{ij}u_j dV - \int_D u_i L_{ij}u_j^* dV \\ &= \int_S \tau_i u_i^* dS - \int_S \tau_j^* u_j dS \end{aligned} \tag{47}$$

and

$$\int_D p^* L_{44} p dV - \int_D p L_{44} p^* dV = \int_S q_n p^* dS - \int_S q_n^* p dS \quad (48)$$

where τ_i and q_n are tractions corresponding to the effective stress and the normal gradient of fluid pressure. They are expressed by using traction operators B_{ij} and B_{44} as follows:

$$\tau_i = B_{ij} u_j = C_{kilj} n_k \partial_l u_j \quad (49)$$

$$q_n = B_{44} p = \frac{1}{\omega^2 \tilde{m}} n_k \partial_k p. \quad (50)$$

For the coupling terms, the following relations are derived

$$\int_D \left(u_i^* L_{i4} p - u_i L_{i4} p^*\right) dV - \int_D \left(p^* L_{4j} u_j - p L_{4j} u_j^*\right) dV = -\tilde{\alpha} \int_S u_j^* p n_j dS + \tilde{\alpha} \int_S p^* u_j n_j dS. \quad (51)$$

Using the definition of $\tilde{\alpha}$ in Eq.(14), we introduce the following traction operators for the coupling terms L_{i4} and L_{4j}

$$v_i = B_{i4} p = -\alpha n_i p \quad (52)$$

$$w_n = B_{4j} u_j = -\frac{\rho_f}{\tilde{m}} n_j u_j. \quad (53)$$

Then Eq.(51) is rewritten as

$$\int_D \left(u_i^* L_{i4} p - u_i L_{i4} p^*\right) dV - \int_D \left(p^* L_{4j} u_j - p L_{4j} u_j^*\right) dV = \int_S u_j^* v_j dS - \int_S u_j v_j^* dS + \int_S p^* w_n dS - \int_S p w_n^* dS. \quad (54)$$

Using the tractions defined above, a traction vector corresponding to the total stress t_i is obtained as

$$t_i = \tau_i + v_i = \sigma_{ij} n_j - \alpha p n_i \quad (55)$$

and the relative fluid motion to the solid frame p_n is obtained as

$$p_n = w_n + q_n = -\frac{\rho_f}{\tilde{m}} u_i n_i + \frac{1}{\omega^2 \tilde{m}} p_{,i} n_i. \quad (56)$$

When $p_{,i}$ in Eq.(56) is replaced with the equation of motion without the body force term

$$p_{,i} = \omega^2 (\rho_f u_i + \tilde{m} w_i) \quad (57)$$

the relative fluid motion p_n is rewritten as

$$p_n = w_n + q_n = w_i n_i. \quad (58)$$

As shown in **Fig.1**, $w_i n_i$ is the fluid volume passing through the unit area of the solid frame. Then if $p_n = w_n + q_n = 0$, the boundary is regarded to be impermeable, and no fluid can move through the surface.

Hereafter, the generalized traction $\boldsymbol{s}$ is introduced as:

$$\boldsymbol{s} = \{t_1,\ t_2,\ t_3,\ p_n\}^T. \quad (59)$$

The reciprocal relation of the total system is written as

$$\int_D q_I^* L_{IJ} q_J dV - \int_D q_I L_{IJ} q_J^* dV = \int_S q_I^* B_{IJ} q_J dS - \int_S q_I B_{IJ} q_J^* dS \quad (60)$$

where the traction operator B_{IJ} is expressed as

$$B_{IJ} = \begin{bmatrix} B_{ij} & B_{i4} \\ B_{4j} & B_{44} \end{bmatrix} = \begin{bmatrix} C_{kilj} n_k \partial_l & -\alpha n_i \\ -\frac{\rho_f}{\tilde{m}} n_j & \frac{1}{\omega^2 \tilde{m}} n_k \partial_k \end{bmatrix}. \quad (61)$$

(2) Scattering problems

For a scattering problem, a single scatterer (D^c) embedded in an infinite and uniform poroelastic media (D) is considered as shown in **Fig.5**. We denote the incident wave as $\boldsymbol{q}^{\mathrm{in}}$ and the scattered wave as $\boldsymbol{q}^{\mathrm{sc}}$.

By substituting the scattering wave q_I^{sc} to q_I and the fundamental solution G_{IK} to q_I^*, Eq.(60) is rearranged as:

$$\int_D \left[G_{IK}(\boldsymbol{x}, \boldsymbol{y}) L_{KJ}^x q_J(\boldsymbol{x}) - q_I(\boldsymbol{x}) L_{IJ}^x G_{JK}(\boldsymbol{x}, \boldsymbol{y})\right] dV_x = \int_S \left[G_{IK}(\boldsymbol{x}, \boldsymbol{y}) B_{KJ}^x q_J(\boldsymbol{x}) - q_I(\boldsymbol{x}) B_{IJ}^x G_{JK}(\boldsymbol{x}, \boldsymbol{y})\right] dS_x \quad (62)$$

Using the definition of the fundamental solution in Eq.(35), the nature of the delta function ($\int f(\boldsymbol{x}) \delta(\boldsymbol{x}, \boldsymbol{y}) dx = f(\boldsymbol{y})$), and the Sommerfeld radiation condition ($\boldsymbol{q}^{\mathrm{sc}}(\boldsymbol{x})|_{|x| \to \infty} = 0$), Eq.(62) is rewritten as

$$C_{KI} q_I^{\mathrm{sc}}(\boldsymbol{y}) = \int_S \left[G_{IK}(\boldsymbol{x}, \boldsymbol{y}) s_I - q_I(\boldsymbol{x}) B_{IJ} G_{JK}(\boldsymbol{x}, \boldsymbol{y})\right] dS \quad (63)$$

where $q_I(\boldsymbol{x})$ and $s_I(\boldsymbol{x})$ define the total displacements and traction fields ($q_I(\boldsymbol{x}) = q_I^{\mathrm{in}}(\boldsymbol{x}) + q_I^{\mathrm{sc}}(\boldsymbol{x})$,

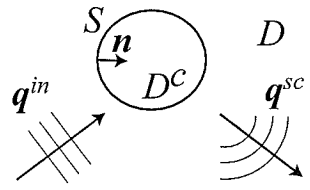

Fig. 5 The scatterer D^c embedded in infinite poroelastic media D

Table 1 Summary of the boundary conditions

type of conditions	given(=0)	unknown
1. Free - Impermeable	$t_i = p_n = 0$	u_i, p
2. Free - Permeable	$t_i = p = 0$	u_i, p_n
3. Fixed - Impermeable	$u_i = p_n = 0$	t_i, p
4. Fixed - Permeable	$u_i = p = 0$	t_i, p_n

and $s_I(\boldsymbol{x}) = s_I^{\text{in}}(\boldsymbol{x}) + s_I^{\text{sc}}(\boldsymbol{x})$). The boundary integral equation for the total field is reduced to the following form

$$C_{KI} q_I(\boldsymbol{x}) = q_K^{\text{in}} + \int_S [G_{KI}(\boldsymbol{x}, \boldsymbol{y}) s_I(\boldsymbol{y}) - W_{KI}(\boldsymbol{x}, \boldsymbol{y}) q_I(\boldsymbol{y})]\, dS \tag{64}$$

where C_{KI} denotes the free term[22),23)] and written as $C_{KI} = \delta_{KI}/2$ on the smooth surface S. The traction vector s_I and the traction kernel W_{KI} are derived as follows

$$s_I(\boldsymbol{y}) = B_{IJ}^y u_J(\boldsymbol{y}) = \{t_i, p_n\}^T \tag{65}$$

$$W_{KI}(\boldsymbol{x}, \boldsymbol{y}) = B_{IJ}^y G_{JK}(\boldsymbol{y}, \boldsymbol{x}) = B_{IJ}^y G_{KJ}(\boldsymbol{x}, \boldsymbol{y}) \tag{66}$$

where B_{IJ}^y is a traction operator acting on the source point $\boldsymbol{y}$. In Eq.(66), the relation for the fundamental solution G_{IK} of poroelasticity

$$G_{IK}(\boldsymbol{x}, \boldsymbol{y}) = G_{KI}(\boldsymbol{y}, \boldsymbol{x}) \tag{67}$$

is used. The explicit form of W_{IJ} is shown in Appendix A.

Eq.(64) and a set of the boundary conditions summarized in **Table 1** and **Fig.6** give a solution on the surface point $\boldsymbol{x}$ on S. In the table and figure, a condition that the solid displacements are fixed ($u_i = 0$) is denoted as *Fixed*, and total traction free condition ($t_i = 0$) is denoted as *Free*. No fluid flux condition ($p_n = 0$) and no pressure condition ($p = 0$) are denoted as *Impermeable* and *Permeable*, respectively.

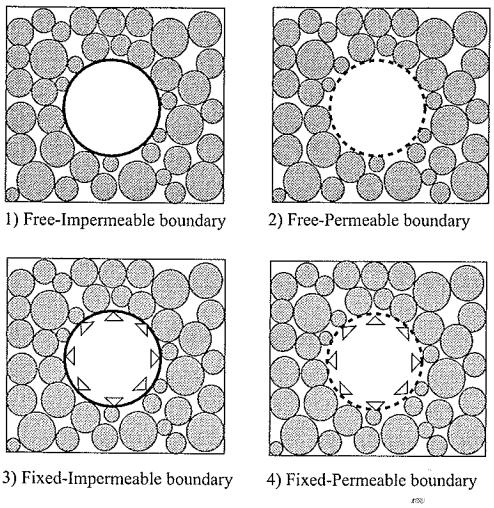

Fig. 6 Schematics of the boundary conditions

5. SCATTERING OF WAVE BY A SPHERICAL SCATTERER

To illustrate some natures of wave scattering in poroelastic media, some numerical results are presented for problems of an $L1$-wave incidence on to a spherical cavity with permeable or impermeable surface.

(1) The setting of the model

A spherical cavity with radius a is shown in **Fig.7**. The surface of the sphere is discretized with the linear quadrilateral and triangular elements. In the spherical coordinates denoted by (r, θ, φ), the pitch of the nodes is chosen as 5 degrees in the θ direction and 30 degrees in the φ direction. The pitch of division of θ direction is determined to ensure the accuracy in high frequency cases, and reduced in φ direction because of the axisymmetry of the system in which values of scattered field are uniform in this coordination. The numerical procedures to solve the boundary integral equation in Eq.(64) are the same as those for the elastic problem, and we follow the procedure described in Refs.[22),23)]

Apparently, the double layer kernels W_{ij}, W_{44} have higher order singularity ($O(r^{-3})$). However the apparent singularity is eliminated by power-series expansion of the kernels as in an elastic problem. Also the sum of the Cauchy singular integral and free term is calculated by considering a rigid body motion as same as the elastic case.[23)]

The incident $L1$-wave has both solid displacements (u_i^{in}) and fluid pressure (p^{in}) components, and propagates along the x_3-axis. The origin of the phase and dissipation is set on the plane

Table 2 poroelastic parameters for the numerical examples

$\mu/(\lambda+2\mu)$	$\lambda/(\lambda+2\mu)$	$M/(\lambda+2\mu)$	β	ρ_f/ρ
1/3	1/3	5/6	0.2	1/3

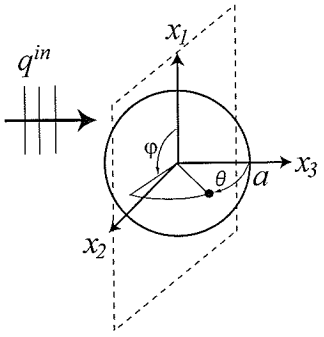

Fig. 7 A spherical cavity with radius a and the incident wave $\boldsymbol{q}^{\mathrm{in}}$.

$x=-a$, so the incident wave $\boldsymbol{q}^{\mathrm{in}}(\boldsymbol{x})$ is written as

$$\boldsymbol{q}^{\mathrm{in}}(\boldsymbol{x}) = \left\{u_1^{\mathrm{in}}, u_2^{\mathrm{in}}, u_3^{\mathrm{in}}, p^{\mathrm{in}}\right\}^T = \left\{0, 0, Ae^{ik_{L1}(x_3+a)}, Be^{ik_{L1}(x_3+a)}\right\}^T. \quad (68)$$

The amplitudes of the displacement and the pressure A and B satisfy Eq.(31). The frequency of the incident wave is indicated by the dimensionless wave number ak_{Ld}.

The dimensionless parameters $\mu/(\lambda+2\mu)$, $\lambda/(\lambda+2\mu)$, $M/(\lambda+2\mu)$, β, and ρ_f/ρ commonly used in all cases are listed in **Table 2**. Those values are chosen for typical sandstones.[5)]

(2) Surface displacement

a) Biot's constant α and coupling effects

The total field ($\boldsymbol{q} = \boldsymbol{q}^{\mathrm{in}} + \boldsymbol{q}^{\mathrm{sc}}$) on the cavity surface is obtained as a numerical solution of Eq.(64).

First, we examine the effect of Biot's constant α for no dissipation ($b/(m\omega) = 0$) case. The poroelastic results are compared with the BEM solutions for elastic solid, the accuracy of which was verified with the analytical solutions of Pao and Mow.[24)]

In **Fig.8** and **Fig.9**, the total fields of displacements and fluid pressure on the cavity surface are shown with respect to the polar angle θ and for different frequencies given by the normalized wavenumber $ak_{Ld} = 0.3$ in low frequency case, and $ak_{Ld} = 1.3$ in intermediate frequency case. The radial and circumferential displacements are normalized by the amplitude of the incident wave ($|u_r|/|\boldsymbol{u}^{\mathrm{in}}|$ and $|u_\theta|/|\boldsymbol{u}^{\mathrm{in}}|$), and the

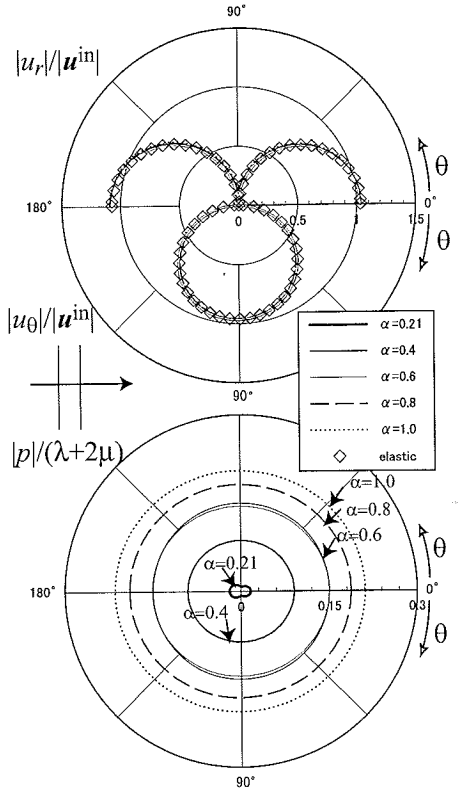

Fig. 8 Surface displacements and pressure on the spherical cavity for different Biot's constants (α=0.21($\approx \beta$), 0.4, 0.6, 0.8 and 1.0). (Low frequecy (ak_{Ld}=0.3). *Free-Impermeable* condition. No dissipation ($b/m\omega = 0$).)

fluid pressure is normalized by the elastic constant $\lambda+2\mu$ ($|p|/(\lambda+2\mu)$). Biot's constant α is set to be 0.21($\simeq \beta = 0.2$) to 1.0. The numerical solutions for the elastic case are depicted by the symbol $\diamond$ in the figures. The boundary condition of *Free-Impermeable* is considered in both cases of $ak_d = 0.3$ and 1.3, while the surface displacements of *Free-Permeable* case is shown only in the intermediate frequency case ($ak_{Ld} = 1.3$).

As the Biot's constant α is closer to the porosity ($\alpha = 0.21 \simeq \beta = 0.2$), the solid displacements in the poroelastic medium converge to the elastic solutions in all cases. The effect of α is mainly seen in the radial displacement ($|u_r|/|\boldsymbol{u}^{\mathrm{in}}|$) and the fluid pressure ($|p|/(\lambda+2\mu)$), especially in the intermediate frequency case. The change of the circumferential displacement ($|u_\theta|/|\boldsymbol{u}^{\mathrm{in}}|$) is slight in all cases. The effect on the surface displacements is clearer in the impermeable surface cases than the permeable cases in which no pore pressure is induced at the surface.

The above discussion suggests that the dis-

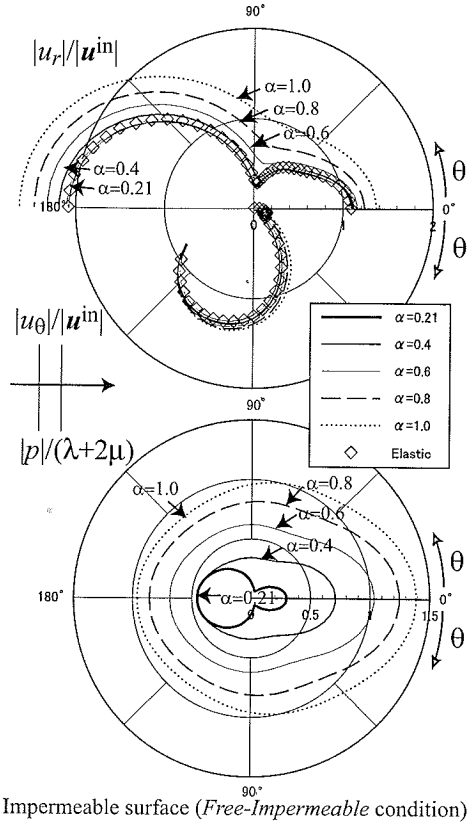

Impermeable surface (*Free-Impermeable* condition)

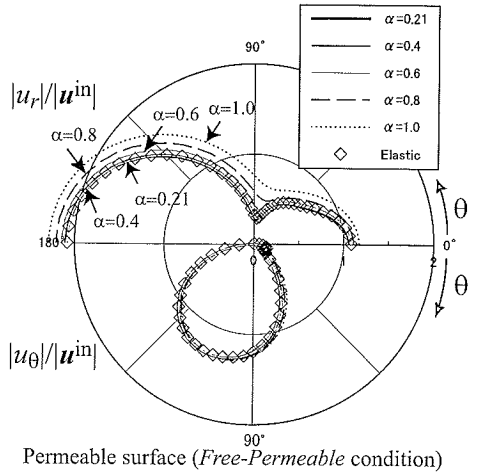

Permeable surface (*Free-Permeable* condition)

Fig. 9 Surface displacements and pressure on the spherical cavity for different Biot's constants (α=0.21($\approx \beta$), 0.4, 0.6, 0.8 and 1.0). (Intermediate frequency (ak_{Ld}=1.3). No dissipation ($b/m\omega = 0$). *Free-Impermeable* (top) and *Free-Permeable* (bottom) conditions.)

placement in a poroelastic medium differs from the elastic solution due to the effect of pore pressure that causes the volumetric deformation of the medium. Therefore, the difference between the results of poroelastic and elastic media is

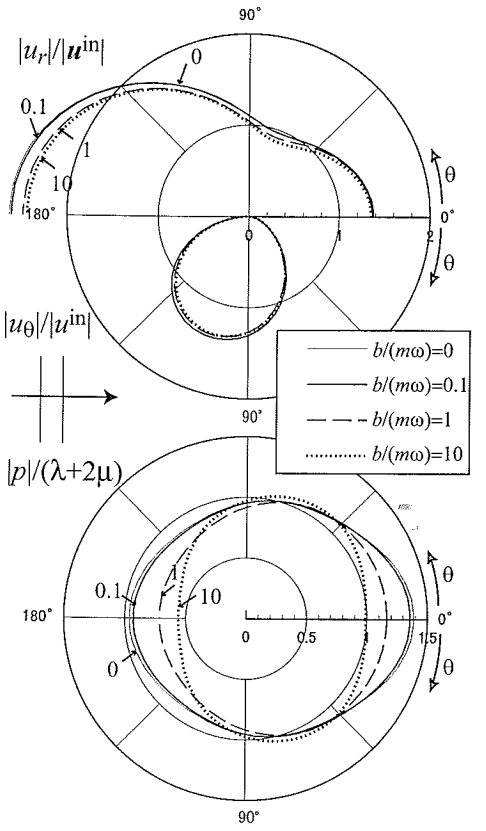

Fig. 10 Surface displacements and pressure on the spherical cavity for different dissipation factors ($b/(m\omega)$=0.01, 0.1, 1.0 and 10.0). (*Free-Impermeable* condition. Intermediate frequency case (ak_{Ld}=1.3). α = 1.0.)

fewer in smaller α cases and permeable surface cases in which the fluid pressure is low.

b) Dissipation factor $b/(m\omega)$

The dimensionless dissipation factor $b/(m\omega)$ is another coupling parameter. The displacements and pressure distribution on the surface are shown in **Fig.10** for various values of the dimensionless dissipation factor ($b/(m\omega)$ =0, 0.1, 1, 10). Biot's constant is set to be one (α = 1.0), and the intermediate frequency (ak_{Ld} = 1.3) and the *Free-Impermeable* condition are used.

The results show that the effect of the dissipation factor $b/(m\omega)$ appears mainly in the distribution of the fluid pressure. The effect on the displacements is slight.

(3) Scattered field near the scatterer

For nondestructive evaluation and geophysical exploration applications, measured data are the amplitudes of scattered waves at a certain position in the medium surrounding the scatterer.

Therefore, distribution of solid displacements and fluid pressure in a surrounding domain is interesting. The effects of Biot's constant α, the boundary condition on the surface (permeable or impermeable), and the dimensionless dissipation factor $b/(m\omega)$ on the scattered field in the medium are examined .

The scattered field $\boldsymbol{q}^{\mathrm{sc}}$ in the domain $D \setminus D^{\mathrm{c}}$ in **Fig.5** is computed by substituting the BEM solutions on the cavity surface into the integral representation of the scattered field, and written as

$$q_K^{\mathrm{sc}}(\boldsymbol{x}) = \int_S [G_{KI}(\boldsymbol{x},\boldsymbol{y}) s_I(\boldsymbol{y}) - W_{KI}(\boldsymbol{x},\boldsymbol{y}) q_I(\boldsymbol{y})]\, dS_y \qquad (69)$$

where $\boldsymbol{x}$ is an observation point. The effects of poroelastic conditions on the scattered fields are investigated by numerical results of Eq.(69) for the following four cases of the media. The dimensionless wavenumber of the incident wave ak_{Ld} is set to be 1.3 (intermediate frequency case).

i) Weakly coupled case. Small Biot's constant ($\alpha = 0.21 (\simeq \beta = 0.2)$), and no dissipation ($b/(m\omega) = 0$) condition is applied. The boundary condition of the cavity surface is *Free-Impermeable*.

ii) Highly coupled case with *Free-Impermeable* condition. Large Biot's constant ($\alpha = 1.0$), and no dissipation ($b/(m\omega) = 0$) condition is applied.

iii) Highly coupled case with *Free-Permeable* condition. Large Biot's constant ($\alpha = 1.0$), and no dissipation ($b/(m\omega) = 0$) condition is applied.

iv) Highly coupled ($\alpha = 1.0$) and high dissipation ($b/(m\omega) = 10$) case with *Free-Impermeable* condition.

The scattered field in x_3-x_1 plane is shown in **Fig.11** and **Fig.12**. The real part of the normalized displacement $\mathrm{Re}(u_3^{\mathrm{sc}})/|\boldsymbol{u}^{\mathrm{in}}|$ and the pressure $\mathrm{Re}(p^{\mathrm{sc}})/(\lambda + 2\mu)$ are plotted in **Fig.11** and **Fig.12**. In the figures, the wavelengthes of $L1$-wave ($\mathrm{Re}(\lambda_{L1})$) and $L2$-wave ($\mathrm{Re}(\lambda_{L2})$) are depicted by arrows.

To observe the difference among the scattered fields for each case more precisely, the absolute value and real part of the scattered fields in the forward ($\theta = 0$) and backward ($\theta = 180$) directions on x_3 axis are shown in **Fig.13** and **Fig.14**, corresponding to **Fig.11** and **Fig.12**. The wavelengths of $L1$-wave ($\mathrm{Re}(\lambda_{L1})$) and $L2$-wave ($\mathrm{Re}(\lambda_{L2})$) are also depicted by arrows in the figures.

It is clear that the coupling parameter α, dissipation factor $b/(m\omega)$, and the surface condition (*Permeable* or *Impermeable*) influence the scattered fields. The effects are clearly seen in the fluid pressure. Alike the pressure on the surface, higher fluid pressure occurs in the highly coupled cases.

By comparing the waveforms of the scattered fields with the wavelengths ($\mathrm{Re}(\lambda_{L1})$ and $\mathrm{Re}(\lambda_{L2})$) at far enough distance from the scatterer, some characters of the scattered fields around the scatterer are found, and summarized as follows:

- In the weakly coupled case, the wavelengths of the solid displacement and pressure are similar to $L1$-wave and $L2$-wave, respectively. This is consistent with the fact that the $L1$-wave is a pure solid wave and the $L2$-wave is a pure pressure wave without the coupling effect. The incident wave does not have an $L2$-wave component, so the observed $L2$-wave is a wave induced by the scattering.

- The distribution of the displacements and pore pressure of highly coupled cases without dissipation are more complex than the weakly coupled case, and the scattered fields seem to contain both $L1$- and $L2$-wave components, as seen clearly in the fluid pressure and in the permeable surface case.

- In the highly dissipated ($b/(m\omega) = 10$) case, the waveform of the pressure is similar to the $L1$-wave, and the $L2$-wave component is not seen in the scattered field.

According to the numerical results, both $L1$- and $L2$-wave components may appear in the scattered field for the $L1$-wave incidence. The conversion of the wave types is known in the refraction of the wave.[25] The numerical results presented here exhibit the wave conversion by the wave scattering. The fluid pressure is highly influenced by the $L2$-wave, then the result of the conversion is seen clearly in the plots of pressure. In the highly dissipated case, however the $L2$-wave component disappears in the scattered fields.

6. CONCLUSION

In this paper, the nature of the scattered field by a scatterer embedded in infinite poroelastic

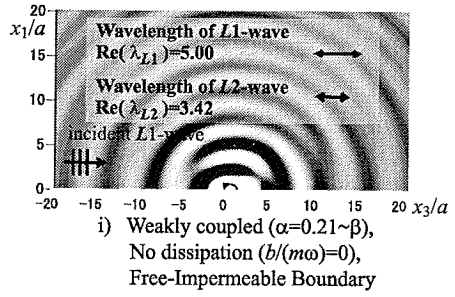

i) Weakly coupled (α=0.21~β),
No dissipation ($b/(m\omega)$=0),
Free-Impermeable Boundary

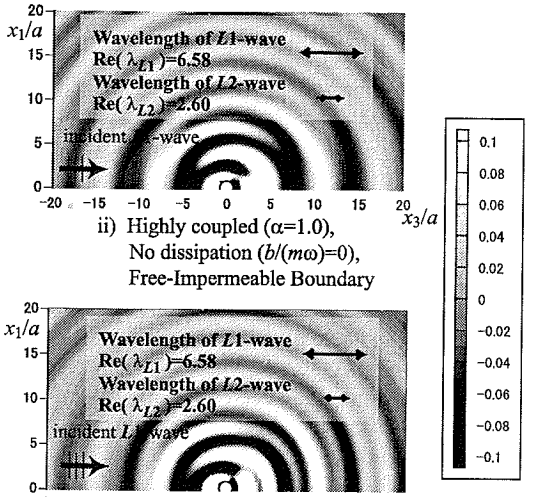

ii) Highly coupled (α=1.0),
No dissipation ($b/(m\omega)$=0),
Free-Impermeable Boundary

iii) Highly coupled (α=1.0),
No dissipation ($b/(m\omega)$=0),
Free-Permeable Boundary

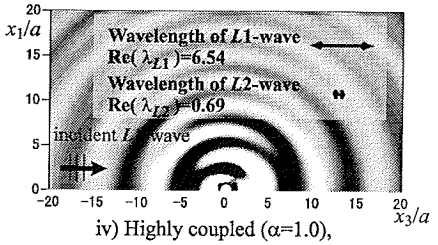

iv) Highly coupled (α=1.0),
High dissipation ($b/(m\omega)$=10),
Free-Impermeable Boundary

$\mathrm{Re}(u_3^{sc})/|u^{in}|$

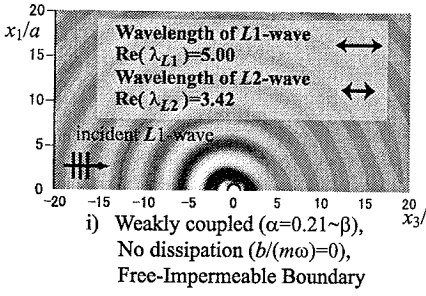

i) Weakly coupled (α=0.21~β),
No dissipation ($b/(m\omega)$=0),
Free-Impermeable Boundary

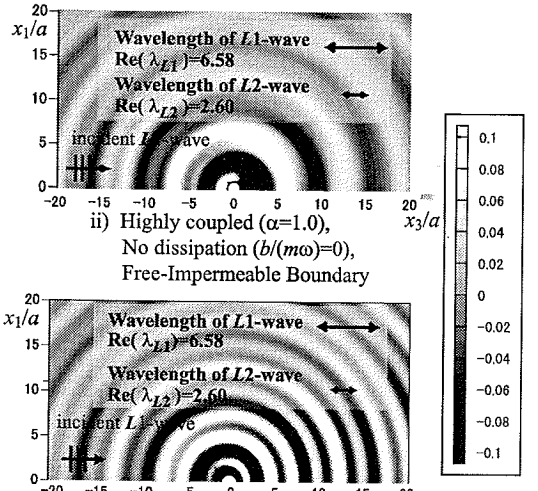

ii) Highly coupled (α=1.0),
No dissipation ($b/(m\omega)$=0),
Free-Impermeable Boundary

iii) Highly coupled (α=1.0),
No dissipation ($b/(m\omega)$=0),
Free-Permeable Boundary

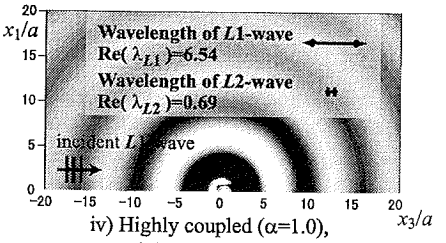

iv) Highly coupled (α=1.0),
High dissipation ($b/(m\omega)$=10),
Free-Impermeable Boundary

$\mathrm{Re}(p^{sc})/H'$

Fig. 11 Distribution of the displacement in the scattered field $Re(u_3^{sc})$ in x_3-x_1 plane.

Fig. 12 Distribution of the pressure in the scattered field $Re(p^{sc})$ in x_3-x_1 plane.

media is investigated. For this purpose, the boundary integral equation is presented for scattering problems by a scatterer in infinite poroelastic media with traction operators for the boundary conditions corresponding to permeable and impermeable surface for the fluid part, and displacement fixed or traction free for the solid part. The three-dimensional fundamental solution for the Biot's material is derived using the Fourier transform.

Some numerical examples are presented for the scattering problem of a longitudinal wave incidence on to a spherical cavity. The total fields on the cavity surface and scattered field in the space near the scatterer are computed. The results show the effects of Biot's constant α, the

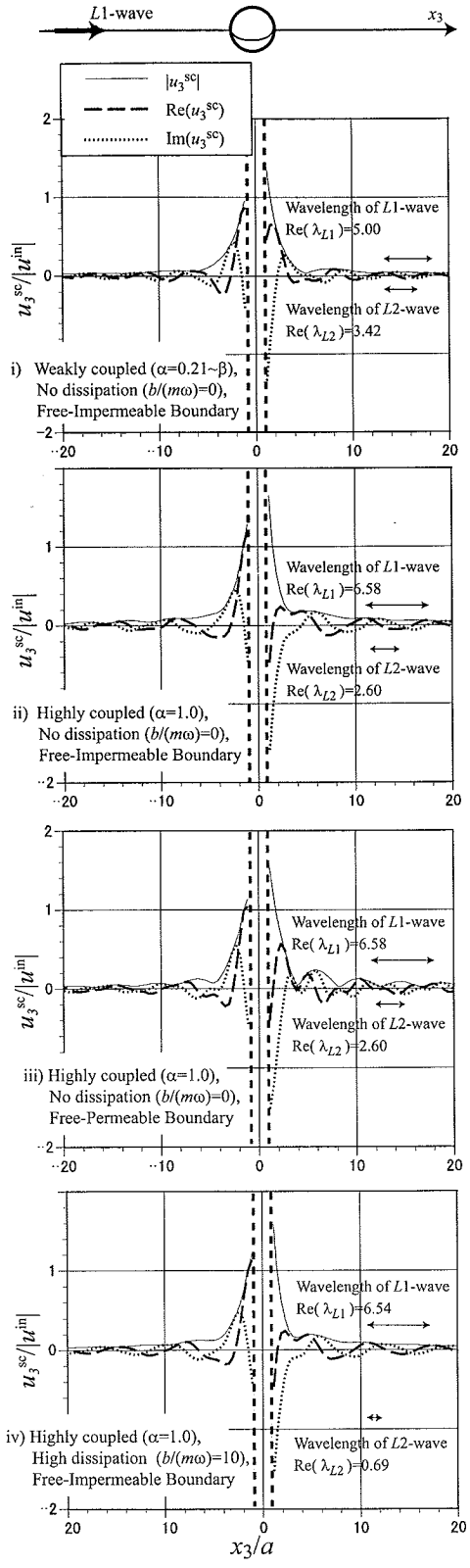

Fig. 13 Distribution of the displacement in the scattered $Re(u_3^{sc})$ on x_3 axis.

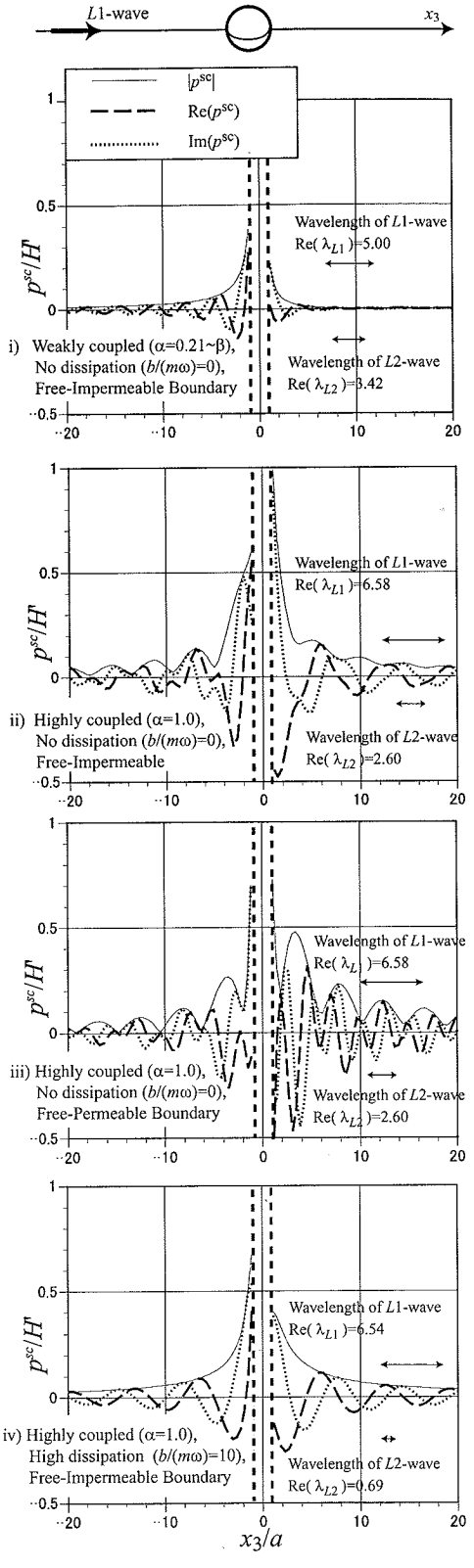

Fig. 14 Distribution of the pressure in the scattered field $Re(p^{sc})$ on x_3 axis.

dissipation factor $b/(m\omega)$, and the boundary condition of the cavity (permeable or impermeable) on the scattered fields.

When α approaches to the porosity β, the coupling effect is negligible, and the poroelastic solutions converge to the elastic solutions. In the highly coupled cases, both $L1$-wave (fast wave) and $L2$-wave (slow wave) appear in the scattered fields around the scatterer by the $L1$-wave incidence. However, the $L2$-wave component disappears soon in the high dissipation case.

The difference between the elastic and poroelastic solutions is caused by coupling effect between the solid and fluid. In other words, the scattered fields contain information on the poroelastic parameters. Especially, the fluid pressure in the scattered field is highly affected by the poroelastic parameters. The conversion between the wave types ($L1$-wave to $L2$-wave and vice versa) is another significant indication of the coupling effect. This phenomena is a cause of variation of fluid pressure in the scattered field.

The results suggest that a scattered field contains information of poroelastic parameters such as Biot's constant α and dissipation factor $b/(m\omega)$ of the media, as well as surface condition of the scatterer. Those effects are observable in waveforms of the scattered wave, then the information from the waveform is useful to identify the characters of the scatterers and surrounding poroelastic media.

To utilize this nature of the scattered field, development of the measurement and data processing techniques of scattered field are necessary, as well as the improvement of the numerical method.

ACKNOWLEDGEMENT: The co-author, Prof. Michihiro Kitahara passed away in the November 8th, 2003. The other author would like to express sincere condolences to the bereaved family. Also the author thanks Prof. Sohichi Hirose for his valuable suggestions on this work.

APPENDIX I DOUBLE LAYER KERNEL

The explicit forms of the double layer kernel W_{IJ} in Eq.(66) are written as follows:

$$
\begin{aligned}
&W_{ij}(\boldsymbol{x},\boldsymbol{y}) = B^y_{jk}G_{ik}(\boldsymbol{x},\boldsymbol{y}) + B^y_{j4}G_{i4}(\boldsymbol{x},\boldsymbol{y})\\
&= -\frac{1}{4\pi}\left[\left\{\frac{\lambda}{\mu}\left(R_3^T + C_4^{TFS}\right) + 2C_1^{TFS}\right\} r_{,i}n_j^y\right.\\
&\quad + \left(R_3^T + C_4^{TFS}\right) r_{,j}n_i^y\\
&\quad + \left\{\left(R_3^T + C_4^{TFS}\right)\delta_{ij} + 2C_2^{TFS} r_{,i}r_{,j}\right\}(r_{,k}n_k^y)\\
&\quad \left. -\frac{\alpha}{\tilde{\alpha}}k_Q^2 K^{12} S_3^{L1;L2} r_{,i}n_j^y\right] \qquad \text{(I.1)}
\end{aligned}
$$

$$
\begin{aligned}
&W_{i4}(\boldsymbol{x},\boldsymbol{y}) = B^y_{4k}G_{ik}(\boldsymbol{x},\boldsymbol{y}) + B^y_{44}G_{i4}(\boldsymbol{x},\boldsymbol{y})\\
&= -\frac{1}{4\pi}\left[\frac{\rho_f}{\tilde{m}}\left(\frac{e^{ik_T r}}{r}n_i^y\right.\right.\\
&\quad + K^{12}\left[L^{L2}\left\{S_5^{T;L2}n_i^y + S_6^{T;L2}(r_{,k}n_k^y)r_{,i}\right\}\right.\\
&\quad \left.\left. - L^{L1}\left\{S_5^{T;L1}n_i^y + S_6^{T;L1}(r_{,k}n_k^y)r_{,i}\right\}\right]\right)\\
&\quad \left. - \frac{\tilde{\alpha}}{\lambda+2\mu}K^{12}\left\{S_5^{L1;L2}n_i^y + S_6^{L1;L2}(r_{,k}n_k^y)r_{,i}\right\}\right] \qquad \text{(I.2)}
\end{aligned}
$$

$$
\begin{aligned}
&W_{4j}(\boldsymbol{x},\boldsymbol{y}) = B^y_{jk}G_{4k}(\boldsymbol{x},\boldsymbol{y}) + B^y_{j4}G_{44}(\boldsymbol{x},\boldsymbol{y})\\
&= \frac{K^{12}}{4\pi}\left(-\frac{k_Q^2}{\tilde{\alpha}}\left[\left\{\lambda\left(-k_{L1}^2\frac{e^{ik_{L1}r}}{r} + k_{L2}^2\frac{e^{ik_{L2}r}}{r}\right)\right.\right.\right.\\
&\quad \left. + 2\mu S_5^{L1;L2}\right\}n_j^y\\
&\quad + 2\mu S_6^{L1;L2}r_{,j}(r_{,k}n_k^y)\Big]\\
&\quad -\alpha M k_{L2_0}^2 n_j^y\\
&\quad \left.\left.\times\left\{(k_{L1_0}^2 - k_{L2}^2)\frac{e^{ik_{L2}r}}{r} - (k_{L1_0}^2 - k_{L1}^2)\frac{e^{ik_{L1}r}}{r}\right\}\right) \qquad \text{(I.3)}
\end{aligned}
$$

$$
\begin{aligned}
&W_{44}(\boldsymbol{x},\boldsymbol{y}) = B^y_{4k}G_{4k}(\boldsymbol{x},\boldsymbol{y}) + B^y_{44}G_{44}(\boldsymbol{x},\boldsymbol{y})\\
&= \frac{K^{12}}{4\pi}\left[-\frac{\rho_f}{\tilde{\alpha}\tilde{m}}k_Q^2(R_3^{L1} - R_3^{L2})\right.\\
&\quad \left. - \left\{(k_{L1_0}^2 - k_{L2}^2)R_3^{L2} - (k_{L1_0}^2 - k_{L1}^2)R_3^{L1}\right\}\right]\\
&\quad \times(r_{,k}n_k^y) \qquad \text{(I.4)}
\end{aligned}
$$

where

$$
R_1^p = \left(\frac{3}{r^3} - \frac{3ik_p}{r^2} - \frac{k_p^2}{r}\right)\frac{e^{ik_p r}}{r}
$$

$$
R_2^p = \left(-\frac{15}{r^3} + \frac{15ik_p}{r^2} + \frac{6k_p^2}{r} - ik_p^3\right)\frac{e^{ik_p r}}{r}
$$

$$
R_3^p = \left(-\frac{1}{r} + ik_p\right)\frac{e^{ik_p r}}{r}
$$

$$
R_4^p = \left(\frac{k_p^2}{r} - ik_p^3\right)\frac{e^{ik_p r}}{r}
$$

$$
R_5^p = \left(-\frac{1}{r^2} + \frac{ik_p}{r}\right)\frac{e^{ik_p r}}{r}
$$

$$
R_6^p = \left(\frac{3}{r^2} - \frac{3ik_p}{r} - k_p^2\right)\frac{e^{ik_p r}}{r}
$$

$$C_1^{TFS} = K^{12}\left\{L^{L2}S_1^{T;L2} - L^{L1}S_1^{T;L1}\right\}$$
$$C_2^{TFS} = K^{12}\left\{L^{L2}S_2^{T;L2} - L^{L1}S_2^{T;L1}\right\}$$
$$C_4^{TFS} = K^{12}\left\{L^{L2}S_4^{T;L2} - L^{L1}S_4^{T;L2}\right\}$$

$$S_1^{p;q} = R_1^p - R_1^q$$
$$S_2^{p;q} = R_2^p - R_2^q$$
$$S_3^{p;q} = R_3^p - R_3^q$$
$$S_4^{p;q} = R_4^p - R_4^q$$
$$S_5^{p;q} = R_5^p - R_5^q$$
$$S_6^{p;q} = R_6^p - R_6^q$$

and

$$L^{L1} = \frac{k_{L1_0}^2 - k_{L2}^2}{k_T^2}$$
$$L^{L2} = \frac{k_{L1_0}^2 - k_{L1}^2}{k_T^2}.$$

REFERENCES

1) Biot, M.A.: General theory of three-dimensional consolidation, *J. Appl. Phys.*, Vol.12, pp.155-164, 1941.
2) Biot, M.A.: Theory of propagation of elastic waves in a fluid-saturated porous solid. I. Low-frequency range, *J. Acoust. Soc. Am.*, Vol.28, pp.168-178, 1956.
3) Biot, M.A.: Mechanics of deformation and acoustic propagation in porous media, *J. Appl. Phys.*, Vol.33, pp.1482-1498, 1962.
4) Yamamoto, T.: Propagation matrix for continuously layered porous seabeds, *Bulletin of Seismological Soc. Am.*, Vol.73, pp.1621-1636, 1983.
5) Detournay, E. and Cheng, A. H.-D.: Fundamental poroelasticity,*Comprehensive Rock Engineering : Principles, Practice, and Projects, Vol. 2 Analysis and Design Methods, eds.* C. Fairhurst, pp.113-171, Pergamon Press, Oxford, 1993.
6) Huyghe, J.: We are all porous media, *Poromechanics* II, *eds.* J.-L. Auriault, et al., Balkema, pp.17-28, 2002.
7) Hassanzadeh, S.: Acoustic modeling in fluid-saturated porous media, *Geophysics*, Vol.56, pp.424-435, 1991.
8) Kazama, M. and Nogami, T.: Dynamic analysis of the saturated two-phase layered media by thin layered element method, *J. Struct. Mech. Earthquake Eng., JSCE*, No.446/I-19, pp.187-196, 1992.
9) Kitamura, Y. and Asai, S.: Formulation of closed-form solutions for green functions of saturated porous media using thin layered elements, *J. Struct. Mech. Earthquake Eng., JSCE*, No.513/I-31, pp.161-167, 1995.
10) Takano, S., Yasui, Y. and Iguchi, M.: Dynamic characteristics of pile groups in fluid-filled poroelastic layers, *Proc. The 10th Japan Earthquake Engineering Symposium*, pp.1941-1946, 1998.
11) Takano, S., Yasui, Y. and Iguchi, M.: Dynamic soil-structure interaction analysis of pile groups in layered fluid-filled poroelastic soil by thin layered element method, *J. Struct. Constr. Eng., AIJ*, No.515, pp.67-74, 1999.
12) Dargush, G. F. and Banerjee, P. K.: A time domain boundary element method for poroelasticity, *Int. J. Numer. Meth. Eng.*, Vol.28, pp.2423-2449, 1989.
13) Cheng, A. H.-D., Badmus, T. and Beskos, D.E.: Integral equation for dynamic poroelasticity in frequency domain with BEM solution, *J. Eng. Mech., ASCE*, Vol.117, pp.1136-1157, 1991.
14) Dominguez, J.: Boundary element approach for dynamic poroelastic problems, *Int. J. Numer. Meth. Eng.*, Vol.35, pp.307-324, 1992.
15) Fukui, T., Funato, K. and Inoue, K.: Frequency domain boundary element method for wave propagation in Biot material, *J. Boundary Element Methods, JASCOME*, Vol.13, pp.149-152, 1996.
16) Utsumi, H., Kawakami, T. and Kitahra, M.: Dynamic distribution of pore water pressures in the seabed around structures, *J. Boundary Element Methods, JASCOME*, Vol.14, pp.1-6, 1997.
17) Kitamura, Y., Amino, H. and Asai, S.: Dynamic analysis of saturated porous elastic soil and fluid system using boundary element method, *The Construction Engineering Research Institute Foundation Report (Kensetsu Kougaku Kenkyujo Houkoku)*, No.35, pp.141-157, 1993.
18) Biot, M.A. and Willis, D.G.: The elastic coefficients of the theory of consolidation, *J. Appl. Mech.*, Vol.24, pp.594-601, 1957.
19) Rice, J.R. and Cleary, M.P.: Some basic stress-diffusion solutions for fluid saturated elastic porous media with compressible constituents, *Rev. Geophys. Space phys.*, Vol.14, pp.227-241, 1977.
20) Stoll, R.D. and Bryan, G.M.: Wave attenuation in saturated sediments, *J. Acoust. Soc. Am.*, Vol.47, pp.1440-1447, 1970.
21) Skempton, A. W.: Effective stress in soils, concrete and rocks, *Proc. Conf. on Pore Pressure and Suction in Soils*, Butterworth, London, pp. 4-16, 1961.
22) Nakagawa, K., Kitahara, M. and Hamada, M.: Applications of boundary integral equation methods to three dimensional elastodynamics, *J. Boundary Element Methods*, Vol.1, pp.163-168, 1984.
23) Kitahara, M., Nakagawa, K., and Achenbach, J. D.: Boundary-integral equation method for elastodynamic scattering by a compact inhomogeneity, *Computational Mech.*, Vol.5, pp.129-144, 1989.
24) Pao, Y.H. and Mow, C.C.: Scattering of plane compressional waves by a spherical obstacle, *J. Appl. phys.*, Vol.34, pp.493-499, 1963.
25) Stoll, R.D. and Kan, T.-K.: Reflection of acoustic waves at a water sediment interface, *J. Acoust. Soc. Am.*, Vol.70, pp.149-157, 1970.

(Received October 17, 2003)

多孔質弾性体における散乱波動場の数値解法

山本晃司・北原道弘

Biot の飽和多孔質弾性体モデルに基づき，無限媒質に散乱体が存在する場合の散乱問題に関して境界積分方程式を定式化した．定式化の過程では，固体変位の固定あるいは全応力に対するトラクションが 0 の境界条件，及び流体が浸透性あるいは非浸透性の境界条件を与えることができるように表面力作用素を定義した．境界要素法による数値計算により，球形の散乱体に平面波を入射させた時の，表面及び散乱体近傍の変位・圧力分布を求め，媒質の多孔質弾性パラメータ，及び表面の浸透性・非浸透性の条件が散乱特性に与える影響を調べた．その結果，散乱体近傍の変位及び圧力の分布は弾性体と異なる挙動を示し，散乱波の波形と各波の波長を比較すると，速い縦波の入射に対して遅い縦波が現れて，間隙圧力に大きな影響を与えることが示された．